ACS OMEGA

http://pubs.acs.org/journal/acsodf

Article

Oxidative Esterification of 5-Hydroxymethylfurfural into Dimethyl 2,5-Furandicarboxylate Using Gamma Alumina-Supported Gold Nanoparticles

Helapiyumi Weerathunga, Sarina Sarina, Huai-Yong Zhu, and Eric R. Waclawik*

Cite This: *ACS Omega* 2021, 6, 4740−4748

Read Online

ACCESS | Metrics & More | Article Recommendations | Supporting Information

ABSTRACT: Gold nanoparticles (Au NPs) supported on a nanostructured gamma alumina (γ-Al_2O_3) fiber can exhibit excellent catalytic activity for the conversion of 5-hydroxymethylfurfural to produce its ester derivative, dimethyl 2,5-furandicarboxylate (FDMC). γ-Al_2O_3 was synthesized using a PEG surfactant to generate oxide fibers that randomly stack together into irregular shapes. The average particle sizes of the Au NPs are 1−6 nm, where the catalytically active Au (111) surface is the exposed facet. This 3D nanocatalyst architecture enhances the 5-hydroxymethylfurfural (HMF) oxidative esterification because HMF reactant molecules can readily diffuse into this fibrous structure and adsorb to active catalytic sites, while ester product molecules can diffuse out. Up to 99% HMF conversion and 90% FDMC selectivity can be obtained at a low reaction temperature of 45 °C, and the catalyst shows excellent recyclability. Increasing the Au content in the catalyst minimizes the requirement of a base for HMF conversion. Thus, the Au NPs supported on γ-Al_2O_3 can drive HMF esterification to FDMC efficiently with high product selectivity under very mild reaction conditions, omitting the need for an additional esterification step of the HMF acid.

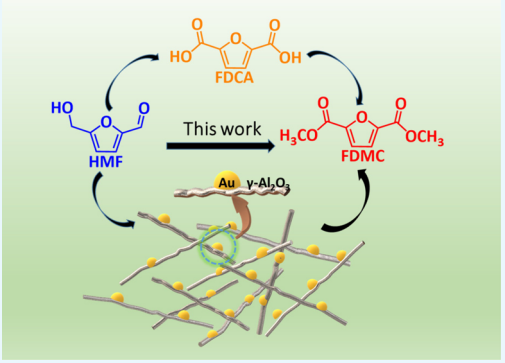

INTRODUCTION

Nonrenewable fossil fuels such as coal, petroleum, and natural gases produce 86% of the world's fuels and 96% of the world's chemicals.[1−3] Large-scale use of fossil fuel energy sources causes significant environment pollution and concerns regarding energy security in the future.[4] With the high availability of renewable carbohydrates in nature (cellulose and other sugars),[5] particular attention has been given to conversion of agricultural waste into value-added chemical commodities.[6] Biomass derivative utilization in the fine chemical and polymer industry has been identified as a potential means to diminish demand for nonrenewable energy sources. Catalytic transformations of biomass derivatives can produce value-added building-block chemicals for the polymer industry and petrol-derived commodities.[7−9] 5-Hydroxymethyl-2-furfural is one biomass-derived platform molecule that is produced from hexoses with treatment of acid catalysts.[10,11] As such, 5-hydroxymethylfurfural (HMF) is a bio-based fuel and a furan ring-based compound that can be catalyst-treated to produce useful product intermediates. HMF having both a hydroxyl group and aldehyde group can react to form value-added high-quality fuel chemicals,[8,12,13] namely, 2,5-dimethylfuran (DMF),[14] 5-ethoxymethylfurfural,[15] ethyl levulinate,[16] and 2,5-furandicarboxylic acid (FDCA).[17]

FDCA has a diacid structure and a furan ring system and is a key ingredient in the polymer industry for synthesis of green, degradable plastics and nontoxic plasticizers.[18] The conventional conversion of HMF into FDCA is done using equivalent oxidizing agents such as nitric acid[19] and potassium hypermanganate.[20] As alternatives, metal/metal oxide nanoparticle systems that use Au,[21] Pd,[22] Ru,[23] and Fe[24] have also been developed to convert HMF into FDCA. FDCA is a solid powder and has a large polarity and a high boiling point[25] with a low solubility in industrial solvents.[26] Extreme acidic and basic conditions are needed to synthesize FDCA, which produces super-stoichiometric inorganic byproducts and has an associated environmental impact.[27] This has led to difficulties in FDCA purification by conventional crystallization and rectification.[28] FDCA is used in the polymer industry in multiple ways. One is by transforming FDCA into its ester prior to transesterification. A second method subjects FDCA to a two-stage polyesterification. The direct polyesterification is considered a better method after comparison, as it omits the additional FDCA esterification step.[29] The direct polyesterification process generates colourless polyesters and has a

Received: November 12, 2020
Accepted: February 2, 2021
Published: February 10, 2021

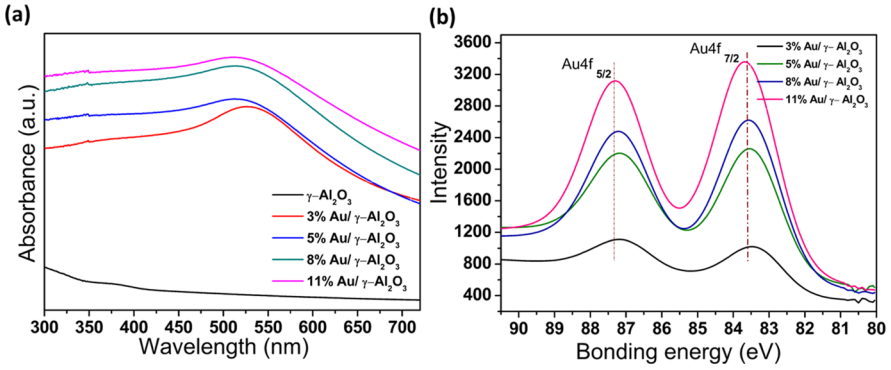

Figure 1. (a) UV−visible spectrum of Au/γ-Al_2O_3 catalysts; (b) XPS spectrum of Au catalysts.

higher reaction rate than when FDCA is used as the starting material. It is also reported that FDCA-derived ester is less decomposed in the polymerization process than FDCA.[30]

Considering all the drawbacks associated with using FDCA, a methyl ester derivative of FDCA, furan-2,5-dimethylcarboxylate (FDMC), may be a useful replacement for FDCA in industry. FDMC is identified as a key intermediate to produce polyethylene furoate.[31] FDMC is readily soluble in most organic solvents. Having a low boiling point, FDMC can readily separate from the reaction mixture and is easily purified.[28] Research on sustainable FDMC production is therefore warranted.[28,32] Most literature reports have demonstrated conversion of HMF in high yields with moderate reaction conditions, but achieving high FDMC product selectivity is challenging using such conditions. It would be desirable to generate catalysts that produce the FDMC product from HMF through one-step oxidative esterification.[32] Au NP catalysts are good candidates for this, due to their remarkable oxidation ability and their resistance to oxygen poisoning.[33] One-step esterification of HMF has been reported using Au NPs supported on a nanoporous polymer host matrix, where the polymer support acted as a conveyor and concentrator of the reactants toward the catalytic sites.[34] A Au−CuO_x nanohybrid catalyst has also been used to obtain FDMC via direct esterification of HMF, where the reaction gave 98% FDMC product selectivity but required comparatively a high reaction temperature of 100−120 °C.[32] Similar high temperature and pressure conditions were used to convert HMF into FDMC using Au on nanoparticulated ceria catalysts (130 °C, 10 bar O_2).[35] 89% of FDMC selectivity has been obtained by hydroxyapatite-supported Au nanocatalysts at 130 °C and 2.4 MPa air pressure.[31] An N-doped carbon-supported CoCu bimetallic catalyst has been able to successfully convert HMF with an FDMC selectivity of 95% at 80 °C without a base using 2 bar of O_2.[36] Another CoRu bimetallic catalyst has been developed by Salazar and co-workers to successfully convert HMF into FDMC with an ester selectivity of 99% using mild temperature and pressure conditions.[37] NaCN-promoted HMF and DFF oxidative esterification has been achieved using MnO_2 metal oxide, which can act as an oxygen regenerator. Here, 83% of the FDMC product was obtained from HMF and 97% FDMC was obtained from DFF.[27] Homogeneous and heterogeneous PdCoBi/C catalysts have been able to convert HMF to FDMC with a 96% ester selectivity using 10 mol % of PdCoBi/C (1:1:1) catalyst at 60 °C with 20% of base.[28] Another work has been reported for HMF oxidative esterification using Au supported on ZrO_2. Au has been supported on sulfated and bare zirconia to investigate the structure dependency for HMF esterification. 100% HMF conversion was obtained with a low FDMC selectivity of 32% using high temperature and pressure conditions.[38]

This study examined how a noble metal-based heterogeneous catalyst can drive the HMF oxidation to obtain FDMC using milder reaction conditions, reduced concentrations of base, lower temperatures, and pressure. This catalyst was prepared by depositing Au nanoparticles on gamma alumina nanofibers using an impregnation precipitation method. Catalysts with different Au loadings were synthesized to optimize the best FDMC yield. 99% HMF conversion and 90% of FDMC selectivity are obtained by this environmentally benign and safe process. A detailed mechanism for the reaction pathway is proposed after studying the effects of the O_2 amount, base, and Au nanoparticle interaction with HMF.

RESULTS AND DISCUSSION

As shown in Figure 1a, the Au/γ-Al_2O_3 catalyst shows a strong light absorbance in the visible and UV range due to the local surface plasmon resonance (LSPR) effect of the Au nanoparticles. The LSPR effect absorption increases with the increase of Au percentage in each catalyst where 11% Au/γ-Al_2O_3 exhibits the highest absorption. A blue shift is observed in the LSPR peak wavelength when the Au loading content increases from 3 to 11%. The γ-Al_2O_3 does not strongly absorb light in these regions, as it absorbs light in the UV region.[39] XPS studies were performed to identify the oxidation state of Au. According to the spectrum shown in Figure 1b, the binding energies for Au $4f_{7/2}$ and Au $4f_{5/2}$ electrons were 83.6 and 87.0 eV, respectively. Accordingly, binding energy intensities for Au $4f_{7/2}$ and Au $4f_{5/2}$ electrons increase when the Au loading increases. These results confirmed that the catalysts were prepared with nanoparticles of Au in their metallic, reduced state.[40] As shown in Figure S1, binding energies for Al 2p are 74.3 and 74.7 eV for γ-Al_2O_3 and 8% Au/γ-Al_2O_3, respectively. The O 1 s peak appears at 531.4 eV for both the Au catalyst and support materials.

Transmission electron microscope studies confirmed the structural properties of the catalyst. The TEM images show the dark, spherical shapes of Au nanoparticles, uniformly dispersed on the γ-Al_2O_3 nanofiber support. As shown in Figure 2, the nanofibers stacked randomly, where the mean length of the fibers is 100 nm and mean width is 4−10 nm. The mean diameter of the reduced Au nanoparticles is 6.46 ± 0.55 nm for 3% Au/γ-Al_2O_3, 5.28 ± 0.79 nm for 5% Au/γ-Al_2O_3, 3.81 ± 0.51 nm for 8% Au/γ-Al_2O_3, and 2.90 ± 0.68 nm for 11% Au/γ-Al_2O_3. The high-resolution TEM image shows the Au nanoparticle spherical shape precisely. As illustrated in Figure

https://dx.doi.org/10.1021/acsomega.0c05541
ACS Omega 2021, 6, 4740−4748

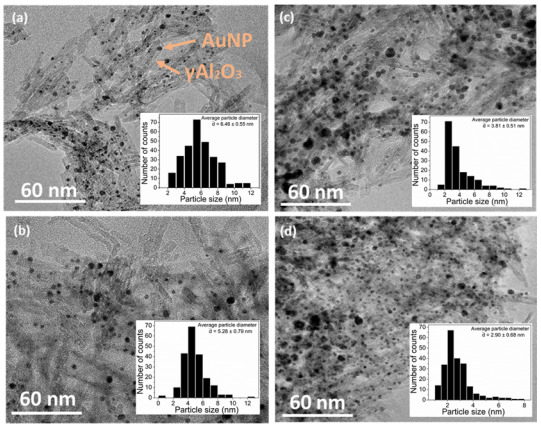

Figure 2. TEM and average particle size histogram of (a) 3% Au/γ-Al_2O_3, (b) 5% Au/γ-Al_2O_3, (c) 8% Au/γ-Al_2O_3, and (d) 11% Au/γ-Al_2O_3 catalysts.

S2, measured *d*-spacings of the Au NPs are 0.235 and 0.203 nm for {111} and {002} planes, respectively. The lattice parameters of the Au NPs can be clearly discerned in Figure S2, characteristic of highly crystalline Au NPs in the form of single nanocrystals, where the Au (111) facet appears to be the principal crystal facet exposed to the environment.

Al_2O_3 can transform into different intermediate crystallographic structures such as χ-, γ-, κ-, δ-, and θ- alumina, depending on the temperature during the process of forming. Out of these forms, γ-Al_2O_3 has an ultrafine, high surface area compared with other phases.[41,42] In this study, the γ-Al_2O_3 support was prepared using the polyethylene glycol surfactant to increase the surface area and volume. The role of the surfactant is to enhance the growth of fibrils by forming rodlike micelles.[43] This highly porous framework structure is identified as an ideal support for catalysts.[44]

XRD patterns obtained for the catalysts are illustrated in Figure 3a. The measured XRD patterns of the powder catalyst samples were compared with entries of the ICDD 2020 PDF-4+ database in Diffrac.EVA v5.2 software and matched with PDF# 048−0367 for the γ-Al_2O_3 crystal phase, where the patterns show identical lattice planes for gamma alumina nanofibers.[45] Au-loaded catalysts were matched with PDF# 066−0091 for the gold crystal phase.[46] The (311), (400), and (440) crystal planes of alumina fibers are preserved by introducing Au NPs into the system. All the metal-loaded catalyst samples show the crystal planes for Au as indicated in Figure S4. The BET equation was used to calculate the specific surface area over a P/P° range of 0.05 to 0.3 for the fiber support and catalysts. As shown in Figure 3, a steep increase from P/P° of 0.7 indicated that all the samples possessed a large volume with a macroporous structure. The gamma alumina gave a BET surface area of 258 m^2/g. The BET values of Au/γ-Al_2O_3 catalysts were 237, 227, 225, and 219 m^2/g for 3% Au/γ-Al_2O_3, 5% Au/γ-Al_2O_3, 8% Au/γ-Al_2O_3, and 11% Au/γ-Al_2O_3, respectively.

As summarized in Table 1, FDMC selectivity increased with an increase in Au NP loading, indicating that the Au nanoparticles are active catalytic centres for HMF oxidation. 99% HMF conversion occurred for all the catalytic samples, but the maximum selectivity toward FDMC occurred with the 8% Au/γ-Al_2O_3 catalyst. When the Au content was increased to 11%, the number density of Au NPs on the support noticeably increased and the Au−Au interparticle distance also decreased, as can be observed in Figure 2 and in Table S1. The FDMC selectivity also decreased for this gold loading. As given in Table S2, when the Au NPs have an average particle size of 3.81 ± 0.51 nm, the best FDMC selectivity was obtained. This could be due to an optimized surface area of active AuNPs exposed for the reaction and Au−Au interparticle distance. A larger number of smaller Au NPs in the system can be one

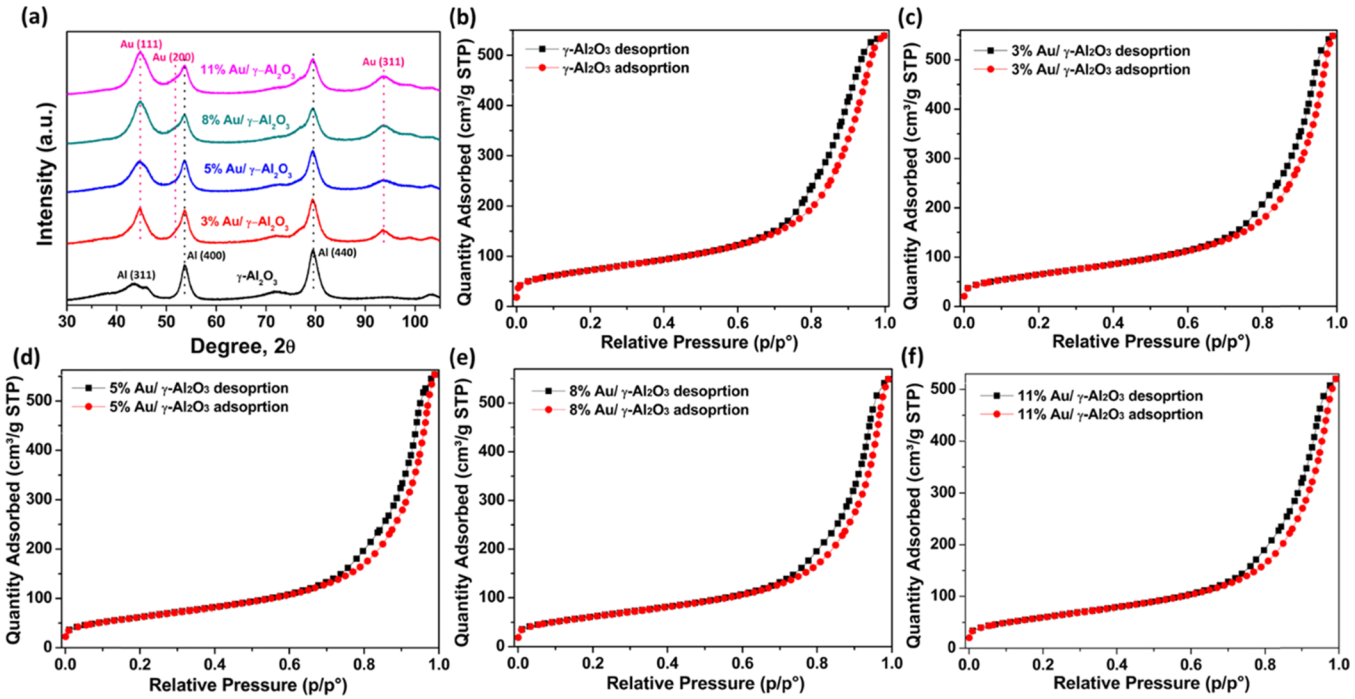

Figure 3. (a) XRD patterns of catalysts and catalyst supports; (b) N_2 adsorption/desorption isotherms of the γ-Al_2O_3 catalyst support, (c) 3% Au/γ-Al_2O_3, (d) 5% Au/γ-Al_2O_3, (e) 8% Au/γ-Al_2O_3, and (f) 11% Au/γ-Al_2O_3 catalysts.

https://dx.doi.org/10.1021/acsomega.0c05541
ACS Omega 2021, 6, 4740−4748

Table 1. Investigating the Effect of Au Loading for HMF Conversion

entry	catalyst	reaction time (h)	HMF conv. (%)	selectivity (%) FDMC	HMFCE
1		16	0		
2	γ-Al_2O_3	16	0		
3	3% Au/γ-Al_2O_3	16	99	45	55
4	5% Au/γ-Al_2O_3	16	99	55	45
5	8% Au/γ-Al_2O_3	16	>99	90	10
6	11% Au/γ-Al_2O_3	16	99	71	29
7	8% Au/70-Al_2O_3	16	68	17	83
8	8% Au/230-Al_2O_3	16	71	36	64
9	8% Au/γ-Al_2O_3	4	90	32	68
10	8% Au/γ-Al_2O_3	8	90	54	46
11	8% Au/γ-Al_2O_3	12	95	72	28
12	8% Au/γ-Al_2O_3	20	>99	90	10

reason for the greater observed FDMC product selectivity and HMF conversion. Control experiments were performed to test for an independent support-only contribution toward the HMF oxidation. As shown in Table 1, no reaction was observed and the γ-Al_2O_3 nanofiber support did not convert HMF in the absence of Au NPs. Any HMF oxidation occurring in the presence of Au NPs is therefore likely to be due to the noble metal active catalytic sites. When in contact with Au NPs, the oxidation of HMF to FDMC can potentially occur by two different reaction paths, depending on the functional group initially oxidized, either the aldehyde group or the hydroxyl functional group can react. From the result summary in Table 1, oxidation of the aldehyde functional group on HMF is favoured by the catalyst system. This results in an intermediate, methyl 5-(hydroxymethyl)furan-2-carboxylate (HMFCE), that converts to FDMC by oxidation of the alcohol. The other reaction pathway that could occur in these conditions would produce 2,5-diformylfuran (DFF) as the intermediate instead, which was not detected in the presence of Au NPs.[47]

Reaction conditions: Methanol (2 mL), HMF (0.2 mmol), KOH (0.1 mmol), catalyst (20 mg), and O_2 (3 min) at 45 °C. 8% Au/70-Al_2O_3 and 8% Au/230-Al_2O_3 = catalysts synthesized by depositing 8% Au on commercially available Al_2O_3 particles with mesh sizes of 70 and 230, respectively.

Catalysts were synthesized by depositing 8% Au on commercially available Al_2O_3 particles with mesh sizes of 70 and 230 to explore how the support material may affect the HMF esterification reaction. Comparing the as-synthesised, nanofiber-supported catalysts with 8% Au/70-Al_2O_3 and 8% Au/230-Al_2O_3 catalysts, low HMF conversion and FDMC product selectivity were obtained. A likely reason is that a reduced surface concentration of basic sites (OH groups) is present on these alumina particle samples compared to γ-Al_2O_3 nanofibers. Basic OH sites on γ-Al_2O_3 fibers play a critical role in the reaction. This difference can be seen in the FT-IR spectra obtained for both γ-Al_2O_3 and Al_2O_3 particles. As illustrated in Figure 4, no OH peaks are visible for Al_2O_3 particles, whereas a clear, broad OH peak was observed for γ-Al_2O_3 fibers.

Reaction time-dependent kinetic behavior of HMF conversion and optimum FDMC product selectivity were investigated. In Table 1, more than 90% HMF converted

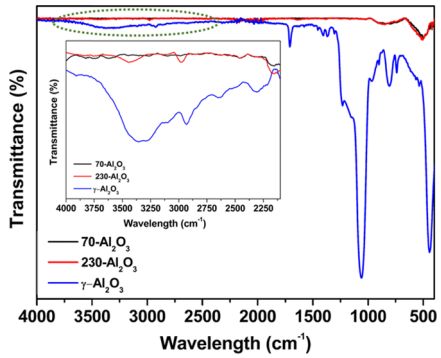

Figure 4. FT-IR spectral comparison between γ-Al_2O_3 and Al_2O_3 particles.

within the first 4 h. FDMC selectivity increased between 4 and 16 h. Higher HMFCE selectivity (also a valuable product) can be obtained after 4 h. FDMC selectivity did not significantly change when the reaction time was increased from 16 to 20 h. The optimized reaction conditions are more than 16 h and less than 12 h to achieve both effective HMF conversion and high FDMC selectivity. These results indicate that HMFCE is the main intermediate formed during HMF oxidative esterification.

Au NPs are stable and effective catalysts for oxidation reactions in the presence of a base.[33] In oxidative esterification, both alkaline strength and alkalinity play an effective role.[28] Green chemistry principles and potential economic advantages dictate the minimization of additives to achieve the same outcomes, where possible. HMF oxidative esterification was performed in methanol at 45 °C using 8% Au/γ-Al_2O_3 as the catalyst. In Table 2, the optimum additive amount is 6 mg (0.1

Table 2. Optimizing Additive Concentration for HMF Oxidation

entry	base	base amount (mmol)	conversion (%)	FDMC selectivity (%)	HMFCE selectivity (%)
1	No base	-	57	28	72
2	KOH	0.01	60	44	56
3	KOH	0.05	73	63	37
4	KOH	0.07	88	75	25
5	KOH	0.08	99	86	14
6	KOH	0.10	99	90	10
7	KOH	0.12	90	77	23
8	KOH	0.14	76	51	49
9	K_2CO_3	0.10	80	56	44
10	LiOH	0.10	90	67	33
11	K-tBuO	0.10	99	72	28

mmol) of KOH. It is important to note that the reaction can also take place in the absence of a base. This implies that Au NPs alone can oxidize 57% of HMF into FDMC, while the base activity promotes further oxidation steps. When increasing the added KOH from 0.01 to 0.14 mmol, the conversion increased and the FDMC selectivity passed through a maximum at 0.10 mmol of KOH added. The selectivity for FDMC drastically drops to 51% when 0.14 mmol mg of base is added. This can be due to the influence of high basicity to FDMC selectivity[48] and HMF gradual degradation (Cannizzaro reaction) at high pH.[49] It has been reported that base concentration significantly influences both HMF oxidation and HMF degradation.[50] When using different base types, the

https://dx.doi.org/10.1021/acsomega.0c05541
ACS Omega 2021, 6, 4740−4748

Scheme 1. HMF Oxidative Esterification Product Selectivity for Different Solvents

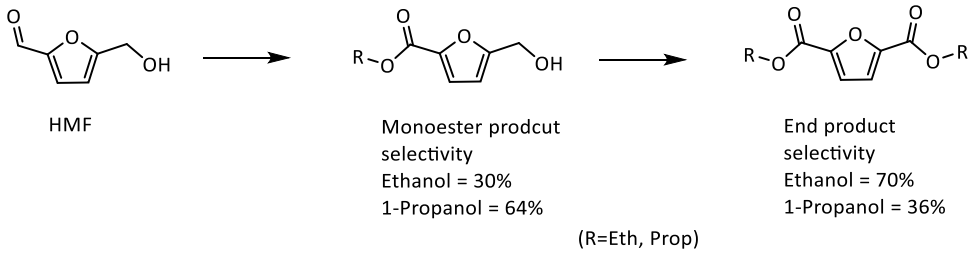

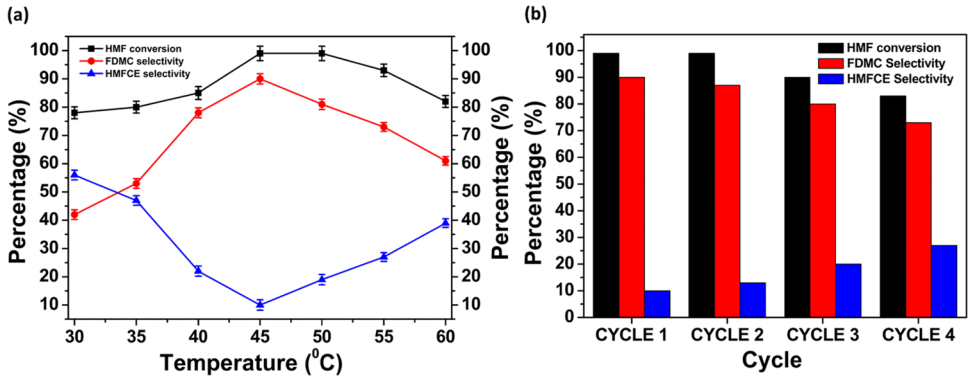

Figure 5. (a) HMF conversion and product selectivity at different temperatures: Methanol (2 mL), HMF (0.2 mmol), KOH (0.1 mmol), 8% Au/γ-Al_2O_3 catalyst (20 mg), O_2 (3 min) for 16 h (b) Reusability of 8% Au/γ-Al_2O_3 catalyst. Reaction conditions: Methanol (2 mL), HMF (0.2 mmol), KOH (0.1 mmol), 8% Au/γ-Al_2O_3 catalyst (20 mg), O_2 (3 min) at 45 °C for 16 h.

Scheme 2. Proposed Reaction Mechanism for HMF Oxidative Esterification to FDMC

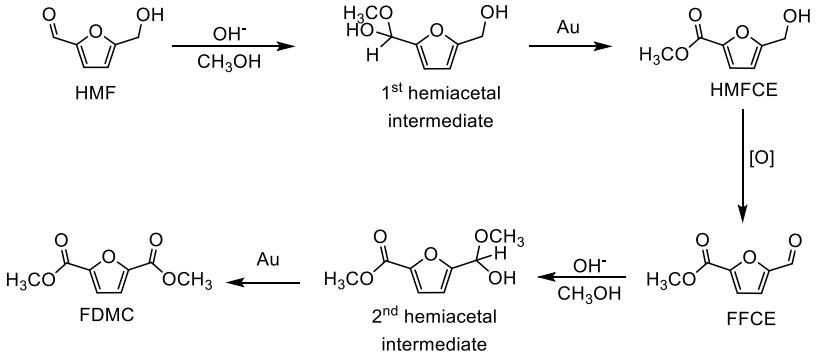

HMF conversion and FDMC selectivity were increased by the alkaline strength. This observation is consistent if a higher pH medium is required to hydrate the aldehyde group into a germinal diol group.[51]

Reaction conditions: Methanol (2 mL), HMF (0.2 mmol), 8% Au/γ-Al_2O_3 catalyst (20 mg), and O_2 (3 min) at 45 °C for 16 h.

One of the essential steps in the esterification of HMF is producing the hemiacetal intermediate, which is subsequently oxidized to the ester. Solvents having different polarities, dielectric constants, steric hindrances, and acid−base properties greatly influence the efficiency of these chemical reactions.[52] Particularly notable is that alcohol solvents having different structural and nucleophilic properties can affect the formation of the hemiacetal intermediate, which in-turn affects the kinetic behavior of the overall reaction. To investigate this phenomenon, different solvents were tested for HMF oxidation under a gold catalyst. Ethanol, 1-propanol, and methanol were solvents that most favored the HMF conversion. The selectivity of HMF conversion to FDMC was higher when using methanol. As illustrated in Scheme 1, with ethanol and 1-propanol as the solvent, two different ester products were obtained. It is therefore likely that during the HMF esterification reaction, the alcohol acted not only as the solvent but also as a substrate molecule that participated in the reaction. When the DMF, DMSO, acetonitrile, and ethyl acetate (all polar aprotic solvents) were used, no reaction occurred, while methanol, 1-propanol, and ethanol, which are polar protic, gave good yields and HMF conversions.

Reactions were carried out under different atmospheres (air, N_2, and O_2) to investigate their influence on HMF oxidation. Only the reaction performed under O_2-containing atmospheres proceeded. It was concluded the oxidant for HMF esterification to FDMC is oxygen. Not needing a continuous flow of oxygen is also a significant factor in this study. It is previously reported that HMF oxidation was greatly influenced by the reaction temperature.[53] As listed in Figure 5a, very low FDMC selectivity was observed when using different reaction temperatures in the range between 30−40 °C. Conversion of HMF and selectivity of dimethyl 2,5-furandicarboxylate ester

https://dx.doi.org/10.1021/acsomega.0c05541
ACS Omega 2021, 6, 4740−4748

increases when increasing the temperature. Although 85% of HMF was converted at 40 °C, the best FDMC selectivity was obtained at 45 °C; the ideal temperature for the reaction was 45 °C, according to Figure 5a. As shown in Figure 5b, a reaction series was carried out to investigate the reusability of the catalyst. Using optimized parameters, four cycles were performed. After each cycle, the catalyst was separated by centrifugation, washed with ethanol, and dried under vacuum at 60 °C for 24 h. The catalyst performed well in the first 3 cycles giving more than 90% of conversion and more than 80% FDMC selectivity. The HMFCE selectivity increased when moving from cycles 1 to 4. The trend of HMF conversion decrease and HMFCE selectivity increase as the cycle number increases is the same as the trend observed when the Au content decreases from 11 to 3%. A gradual decrease of yield can be due to loss of catalyst in the treatment process. No morphological changes of the catalyst were observed after the final run as illustrated in Figure S3.

Following the evolution of the reaction with time, one intermediate compound was detected by GC and GC−MS, which is the monoester primary, unstable product. Considering the kinetic behavior, a possible reaction pathway is given in Scheme 2. Considering the kinetic profiles (Table 1), the only intermediate product obtained in the reaction pathway was HMFCE. The other possible intermediate DFF (2,5-furandicarbaldehyde) was not detected from GC analysis. This suggests that the main reaction pathway for oxidative esterification of HMF to FDMC is path A (Scheme S1).

The catalytic oxidation of aldehyde function is faster than that of alcohol over Au.[54−56] This concludes that the rate-limiting step in the overall reaction is converting HMFCE to FDMC. A methoxy group is formed by proton abstraction by the base or basic sites of γ-Al_2O_3. By the reaction between the methoxy group and aldehyde on HMF, the first hemiacetal intermediate will form. Au will abstract the H in the α C−H bond of the hemiacetal intermediate.[57] This unstable intermediate will immediately convert to the monoester product (HMFCE detected by GC and GC−MS) via a β hydrogen elimination reaction on the Au active catalytic site. This was confirmed by the data from Table 2, where 57% HMF conversion and 72% HMFCE selectivity were obtained without using a base. Electron transfer from negatively charged Au to O_2 will generate activated oxygen species.[58−60] The molecular oxygen will oxidize the primary alcohol group in HMFCE to aldehyde forming methyl 5-formylfuran-2-carboxylate (FFCE). FFCE is attacked again by a methoxy group to form the 2nd hemiacetal intermediate. As in the last step, the 2nd hemiacetal intermediate will turn into FDMC via a β hydrogen elimination reaction. This suggests that both the base and γ-Al_2O_3 promote the HMF esterification to FDMC on Au NP active catalytic sites. It is important to note that the product distribution highly depends on pH. Finally, the surface-adsorbed H atoms in Au nanoparticles will be removed by O_2 (no need of atomic oxygen[57]) as water.[61] The gamma alumina fibers not only act as a support but will also promote the reaction by providing basic sites.

CONCLUSIONS

Here, we report an efficient direct oxidation route to synthesize dimethyl-2,5-furandicarboxylate from 5-hydroxymethylfurfuryl. γ-Al_2O_3 fibers act as a reliable and a cheap catalyst support for heterogeneous Au NP catalysts and shows promising results for conversion of HMF to its derivative ester and selectivity, under remarkably mild conditions, having only one intermediate product in the synthesis mechanism. The catalyst can readily isolate FDMC ester without further oxidation to its acid or CO_2. A low stoichiometric amount of an inorganic base (HMF/base 2:1 mmol) used with moderate temperature is another key feature of the transformation. The AuNP catalyst converts more than 50% of HMF with a 20% product selectivity of the ester, even with the absence of the base. The byproduct HMFCE is a valuable intermediate produced with more than 70% selectivity within the first 4 h with this method. The 3D nanocatalyst architecture enhances the HMF oxidative esterification, since HMF reactant molecules can readily diffuse in this fiber structure and adsorb to the active catalytic sites, while ester product molecules can diffuse out. Advantages to using this catalyst material include efficient conversion to products using a minimum amount of base and mild reaction conditions favored by the green synthesis.

EXPERIMENTAL SECTION

Materials. The listed chemicals were purchased from given commercial suppliers: 5-(hydroxymethyl)furfural (Sigma-Aldrich, >99%), isopropanol (Sigma-Aldrich, >99.5%,anhydrous), methanol (Sigma-Aldrich, HPLC), ethanol (Sigma-Aldrich, >99%), ethyl acetate (Sigma-Aldrich, >99%), *N*,*N*-dimethyl formamide (Sigma-Aldrich, >99.8%, anhydrous), toluene (Fisher, >99.99%, GC assay), acetic acid (Ajax Finechem, >99.7%), $C_{12\text{-}14}H_{25\text{-}29O}(CH_2CH_2O)_5H$ surfactant (Sigma-Aldrich), potassium hydroxide (Sigma-Aldrich, >99.99%), lithium hydroxide (Sigma-Aldrich, >99.99%), potassium *tert*-butoxide (Sigma-Aldrich, >99.99%), potassium carbonate (Sigma-Aldrich, >99.99%), gold chloride trihydrate (Sigma-Aldrich, >99.9%), sodium borohydride (Sigma-Aldrich, >98%), sodium aluminate (Sigma-Aldrich, anhydrous), and 0_2 (Supagas, >99.999%).

Synthesis of γ-Al_2O_3 Nanofibers. γ-Al_2O_3 was synthesized using a previously reported method.[62] $NaAlO_2$ (18.81 g) was dissolved in 50 mL of distilled water. This suspension was stirred at room temperature to obtain a homogeneous mixture. This solution was added to 50 mL of 5 M acetic acid solution dropwise with vigorous stirring. The solution pH was adjusted to approximately 5. A white aluminium hydrate was obtained, washed with water, and recovered by centrifugation (6000 rpm for 20 min). Polyethylene glycol (40 g) was then mixed with the white precipitate, and the mixture was stirred for 1 h. This homogeneous mixture was transferred into a glass bottle and kept at 373 k. Every two days, the first three steps were repeated to synthesize a hydrate cake, which was added to the bottle. After 8 days of this procedure, the mixture was calcined in a muffle furnace for 5 h at 450 °C (obtained γ-Al_2O_3 nanofiber mass − 21.83 g).

Loading Au NPs on γ-Al_2O_3 Nanofibers. γ-Al_2O_3 (1.0 g) was dispersed in 100 mL of distilled water. 3% gold-loaded samples were prepared by the following procedure. 0.01 M $HAuCl_4$ solution (12 mL) was added to the solution. 0.1 M L-lysine was added to achieve a solution pH of 7. Subsequently, 0.35 M $NaBH_4$ was added to the mixture dropwise while stirring. The solution was aged 24 h, and then, the solid was recovered by centrifugation. The Au/γ-Al_2O_3 samples were washed with distilled water (5 times) and ethanol (2 times) and dried overnight at 60 °C in a vacuum oven. Catalysts with four different gold loadings (3, 5, 8, and 11%) were prepared.

Characterization of Catalysts and Supports. Nanoparticles were imaged using a JEOL TEM-2100 transmission

https://dx.doi.org/10.1021/acsomega.0c05541
ACS Omega 2021, 6, 4740−4748

electron microscope with an accelerating voltage of 200 kV. Finely powdered specimens were deposited onto a Cu microgrid coated with a holey carbon film. Surface areas of γ-Al_2O_3 nanofiber samples and catalysts were measured with a Tristar II 3020 isotherm analyzer. The samples were degassed using a VacPrep 061 sample degas system at 250 °C in a vacuum at 100 mTorr for 16 h prior to measurement. The sample's elemental compositions were determined using the energy-dispersive X-ray spectroscopy attachment of an FEI Quanta 200 scanning electron microscope. Diffuse reflectance UV−visible spectra of the samples were also recorded on a Cary 5000 spectrometer. XRD was done to identify the alumina catalyst support's crystal phase. A Bruker D8 advance diffractometer was operated at 35 kV and 40 mA with a Co Kα radiation λ of 0.178 nm. The samples were analyzed with a step size of 0.02° and at a scan range of 20−119°.

General Procedure for the HMF Oxidation Reaction. Reactions were conducted in sealed reaction tubes maintained at 45 °C. 0.2 mmol of HMF, 0.1 mmol of base, 2.0 mL of methanol, and 20 mg of catalyst were placed in a 20 mL glass tube. Prior to the reaction, O_2 gas was purged for 3 min to the reaction mixture. The tubes were then sealed thoroughly. 1 mL aliquots were collected at given time periods. These samples were filtered through a millipore filter (pore size 0.45 μm) to remove the catalyst particulates to analyze products. Reactant conversion and product selectivity were calculated from gas chromatography (GC-HP6890 Agilent Technologies) measurements using a HP-5 column. Product compositions were analyzed using an Agilent HP5973 mass spectrometer.

■ ASSOCIATED CONTENT

Supporting Information

The Supporting Information is available free of charge at https://pubs.acs.org/doi/10.1021/acsomega.0c05541.

(Figure S1) XPS sipectra of catalyst supports and catalysts (other main elements); (Figure S2) gold nanoparticle D spacing values under HRTEM; (Table S1) Au−Au average interparticle distance; (Table S2) average particle sizes of synthesized catalysts and FDMC product selectivity; (Scheme S1) possible reaction pathways for HMF oxidative esterification; (Figure S3) TEM image of the catalyst after the recycle test; and (Figure S4) comparison of XRD spectra for catalysts and catalyst supports (PDF)

■ AUTHOR INFORMATION

Corresponding Author

Eric R. Waclawik − *School of Chemistry and Physics, Queensland University of Technology, Brisbane, Queensland 4000, Australia;* orcid.org/0000-0003-3276-0365; Email: e.waclawik@qut.edu.au

Authors

Helapiyumi Weerathunga − *School of Chemistry and Physics, Queensland University of Technology, Brisbane, Queensland 4000, Australia*

Sarina Sarina − *School of Chemistry and Physics, Queensland University of Technology, Brisbane, Queensland 4000, Australia;* orcid.org/0000-0003-1559-0456

Huai-Yong Zhu − *School of Chemistry and Physics, Queensland University of Technology, Brisbane, Queensland 4000, Australia;* orcid.org/0000-0002-1790-1599

Complete contact information is available at: https://pubs.acs.org/10.1021/acsomega.0c05541

Author Contributions

H.W. − Conceptualization, methodology, validation, formal analysis, investigation, writing, and visualization. S.S.− Methodology, validation, resources, supervision, review, and editing. H.-Y.Z. − Methodology, resources, review and editing, and funding acquisition. E.W. − Methodology, resources, review and editing, supervision, project administration, and funding acquisition.

Funding

Australian Research Council (DP200102652 and DE190101450).

Notes

The authors declare no competing financial interest.

■ ACKNOWLEDGMENTS

The authors acknowledge funding from the Australian Research Council (DP200102652, DP200102652, and DE190101450). The authors would also like to thank the Central Analytical Research Facility (CARF at Queensland University of Technology (QUT)). QUTPRA scholarship was acknowledged by H.W.

■ ABBREVIATIONS

HMF	5-Hydroxymethylfurfural
HMFCE	Methyl 5-(hydroxymethyl)furan-2-carboxylate
FDMC	Dimethyl furan-2,5-dicarboxylate
Au NPs	Gold nanoparticles

■ REFERENCES

(1) Alonso, D. M.; Wettstein, S. G.; Dumesic, J. A. Gamma-valerolactone, a sustainable platform molecule derived from lignocellulosic biomass. *Green Chem.* **2013**, *15*, 584−595.

(2) Binder, J. B.; Raines, R. T. Simple chemical transformation of lignocellulosic biomass into furans for fuels and chemicals. *J. Am. Chem. Soc.* **2009**, *131*, 1979−1985.

(3) Huber, G. W.; Iborra, S.; Corma, A. Synthesis of transportation fuels from biomass: chemistry, catalysts, and engineering. *Chem. Rev.* **2006**, *106*, 4044−4098.

(4) Bruijnincx, P. C. A.; Weckhuysen, B. M. Lignin up for break-down. *Nat. Chem.* **2014**, *6*, 1035−1036.

(5) Zhu, H.; Luo, W.; Ciesielski, P. N.; Fang, Z.; Zhu, J.; Henriksson, G.; Himmel, M. E.; Hu, L. Wood-derived materials for green electronics, biological devices, and energy applications. *Chem. Rev.* **2016**, *116*, 9305−9374.

(6) Eerhart, A.; Huijgen, W.; Grisel, R.; Van der Waal, J.; De Jong, E.; de Sousa Dias, A.; Faaij, A.; Patel, M. K. Fuels and plastics from lignocellulosic biomass via the furan pathway; a technical analysis. *RSC Adv.* **2014**, *4*, 3536−3549.

(7) Budroni, G.; Corma, A. Gold and gold−platinum as active and selective catalyst for biomass conversion: Synthesis of γ-butyrolactone and one-pot synthesis of pyrrolidone. *J. Catal.* **2008**, *257*, 403−408.

(8) Corma, A.; Iborra, S.; Velty, A. Chemical routes for the transformation of biomass into chemicals. *Chem. Rev.* **2007**, *107*, 2411−2502.

(9) Mäki-Arvela, P.; Holmbom, B.; Salmi, T.; Murzin, D. Y. Recent progress in synthesis of fine and specialty chemicals from wood and other biomass by heterogeneous catalytic processes. *Catal. Rev.* **2007**, *49*, 197−340.

(10) Saha, B.; Abu-Omar, M. M. Advances in 5-hydroxymethylfurfural production from biomass in biphasic solvents. *Green Chem.* **2014**, *16*, 24−38.

(11) Qi, X.; Zhou, R.; Ai, H.-J.; Wu, X.-F. HMF and furfural: Promising platform molecules in rhodium-catalyzed carbonylation reactions for the synthesis of furfuryl esters and tertiary amides. *J. Catal.* **2020**, *381*, 215−221.
(12) Bozell, J. J.; Petersen, G. R. Technology development for the production of biobased products from biorefinery carbohydrates—the US Department of Energy's "Top 10" revisited. *Green Chem.* **2010**, *12*, 539−554.
(13) Zhang, Z.; Deng, K. Recent advances in the catalytic synthesis of 2, 5-furandicarboxylic acid and its derivatives. *ACS Catal.* **2015**, *5*, 6529−6544.
(14) Román-Leshkov, Y.; Barrett, C. J.; Liu, Z. Y.; Dumesic, J. A. Production of dimethylfuran for liquid fuels from biomass-derived carbohydrates. *Nature* **2007**, *447*, 982−985.
(15) Lewis, J. D.; Van de Vyver, S.; Crisci, A. J.; Gunther, W. R.; Michaelis, V. K.; Griffin, R. G.; Román-Leshkov, Y.; Continuous Flow, A. Strategy for the Coupled Transfer Hydrogenation and Etherification of 5-(Hydroxymethyl) furfural using Lewis Acid Zeolites. *ChemSusChem* **2014**, *7*, 2255−2265.
(16) Tang, X.; Sun, Y.; Zeng, X.; Hao, W.; Lin, L.; Liu, S. Novel process for the extraction of ethyl levulinate by toluene with less humins from the ethanolysis products of carbohydrates. *Energy Fuels* **2014**, *28*, 4251−4255.
(17) Artz, J.; Palkovits, R. Base-free aqueous-phase oxidation of 5-hydroxymethylfurfural over ruthenium catalysts supported on covalent triazine frameworks. *ChemSusChem* **2015**, *8*, 3832−3838.
(18) Wu, B.; Xu, Y.; Bu, Z.; Wu, L.; Li, B.-G.; Dubois, P. Biobased poly (butylene 2, 5-furandicarboxylate) and poly (butylene adipate-co-butylene 2, 5-furandicarboxylate) s: From synthesis using highly purified 2, 5-furandicarboxylic acid to thermo-mechanical properties. *Polymer* **2014**, *55*, 3648−3655.
(19) El Hajj, T.; Masroua, A.; Martin, J.-C.; Descotes, G. Synthèse de l'hydroxyméthyl-5 furanne carboxaldéhyde-2 et de ses dérivés par traitement acide de sucres sur résines échangeuses d'ions. *Bull. Soc. Chim. Fr.* **1987**, 855−860.
(20) Miura, T.; Kakinuma, H.; Kawano, T.; Matsuhisa, H., *Method for producing furan-2, 5-dicarboxylic acid.* Google Patents : 2008.
(21) Gorbanev, Y. Y.; Klitgaard, S. K.; Woodley, J. M.; Christensen, C. H.; Riisager, A. Gold-catalyzed aerobic oxidation of 5-hydroxymethylfurfural in water at ambient temperature. *ChemSusChem* **2009**, *2*, 672−675.
(22) Liu, X.; Zhang, Z.; Yang, Y.; Yin, D.; Su, S.; Lei, D.; Yang, J. Selective hydrogenation of citral to 3, 7-dimethyloctanal over activated carbon supported nano-palladium under atmospheric pressure. *Chem. Eng. J.* **2015**, *263*, 290−298.
(23) Yi, G.; Teong, S. P.; Zhang, Y. Base-free conversion of 5-hydroxymethylfurfural to 2, 5-furandicarboxylic acid over a Ru/C catalyst. *Green Chem.* **2016**, *18*, 979−983.
(24) Saha, B.; Gupta, D.; Abu-Omar, M. M.; Modak, A.; Bhaumik, A. Porphyrin-based porous organic polymer-supported iron (III) catalyst for efficient aerobic oxidation of 5-hydroxymethyl-furfural into 2, 5-furandicarboxylic acid. *J. Catal.* **2013**, *299*, 316−320.
(25) Sajid, M.; Zhao, X.; Liu, D. Production of 2, 5-furandicarboxylic acid (FDCA) from 5-hydroxymethylfurfural (HMF): recent progress focusing on the chemical-catalytic routes. *Green Chem.* **2018**, *20*, 5427−5453.
(26) Weissermel, K.; Arpe, H.-J., *Industrial organic chemistry*. John Wiley & Sons: 2008.
(27) Kozlov, K. S.; Romashov, L. V.; Ananikov, V. P. A tunable precious metal-free system for selective oxidative esterification of biobased 5-(hydroxymethyl) furfural. *Green Chem.* **2019**, *21*, 3464−3468.
(28) Li, F.; Li, X.-L.; Li, C.; Shi, J.; Fu, Y. Aerobic oxidative esterification of 5-hydroxymethylfurfural to dimethyl furan-2, 5-dicarboxylate by using homogeneous and heterogeneous PdCoBi/C catalysts under atmospheric oxygen. *Green Chem.* **2018**, *20*, 3050−3058.
(29) Sousa, A. F.; Vilela, C.; Fonseca, A. C.; Matos, M.; Freire, C. S.; Gruter, G.-J. M.; Coelho, J. F.; Silvestre, A. J. Biobased polyesters and other polymers from 2, 5-furandicarboxylic acid: a tribute to furan excellency. *Polym. Chem.* **2015**, *6*, 5961−5983.
(30) M Gruter, G.-J.; Sipos, L.; Adrianus Dam, M. Accelerating research into bio-based FDCA-polyesters by using small scale parallel film reactors. *Comb. Chem. High Throughput Screening* **2012**, *15*, 180−188.
(31) Mishra, D. K.; Cho, J. K.; Yi, Y.; Lee, H. J.; Kim, Y. J. Hydroxyapatite supported gold nanocatalyst for base-free oxidative esterification of 5-hydroxymethyl-2-furfural to 2, 5-furan dimethylcarboxylate with air as oxidant. *J. Ind. Eng. Chem.* **2019**, *70*, 338−345.
(32) Du, J.; Fang, H.; Qu, H.; Zhang, J.; Duan, X.; Yuan, Y. Fabrication of supported Au-CuO_x nanohybrids by reduction-oxidation strategy for efficient oxidative esterification of 5-hydroxymethyl-2-furfural into dimethyl furan-2, 5-dicarboxylate. *Appl. Catal. A: Gen.* **2018**, *567*, 80−89.
(33) Prüße, U.; Herrmann, M.; Baatz, C.; Decker, N. Gold-catalyzed selective glucose oxidation at high glucose concentrations and oxygen partial pressures. *Appl. Catal. A: Gen.* **2011**, *406*, 89−93.
(34) Buonerba, A.; Impemba, S.; Litta, A. D.; Capacchione, C.; Milione, S.; Grassi, A. Aerobic Oxidation and Oxidative Esterification of 5-Hydroxymethylfurfural by Gold Nanoparticles Supported on Nanoporous Polymer Host Matrix. *ChemSusChem* **2018**, *11*, 3139−3149.
(35) Casanova, O.; Iborra, S.; Corma, A. Biomass into chemicals: One pot-base free oxidative esterification of 5-hydroxymethyl-2-furfural into 2, 5-dimethylfuroate with gold on nanoparticulated ceria. *J. Catal.* **2009**, *265*, 109−116.
(36) Liu, H.; Ding, N.; Wei, J.; Tang, X.; Zeng, X.; Sun, Y.; Lei, T.; Fang, H.; Li, T.; Lin, L. Oxidative Esterification of 5-Hydroxymethylfurfural with an N-doped Carbon-supported CoCu Bimetallic Catalyst. *ChemSusChem* **2020**, *13*, 4151−4158.
(37) Salazar, A.; Hünemörder, P.; Rabeah, J.; Quade, A.; Jagadeesh, R. V.; Mejia, E. Synergetic Bimetallic Oxidative Esterification of 5-Hydroxymethylfurfural under Mild Conditions. *ACS Sustainable Chem. Eng.* **2019**, *7*, 12061−12068.
(38) Menegazzo, F.; Signoretto, M.; Marchese, D.; Pinna, F.; Manzoli, M. Structure−activity relationships of Au/ZrO_2 catalysts for 5-hydroxymethylfurfural oxidative esterification: Effects of zirconia sulphation on gold dispersion, position and shape. *J. Catal.* **2015**, *326*, 1−8.
(39) Prashanth, P.; Raveendra, R.; Hari Krishna, R.; Ananda, S.; Bhagya, N.; Nagabhushana, B.; Lingaraju, K.; Raja Naika, H. Synthesis, characterizations, antibacterial and photoluminescence studies of solution combustion-derived α-Al_2O_3 nanoparticles. *J. Asian Ceram. Soc.* **2015**, *3*, 345−351.
(40) Zhu, H.; Ke, X.; Yang, X.; Sarina, S.; Liu, H. Reduction of nitroaromatic compounds on supported gold nanoparticles by visible and ultraviolet light. *Angew. Chem., Int. Ed.* **2010**, *49*, 9657−9661.
(41) Favaro, L.; Boumaza, A.; Roy, P.; Lédion, J.; Sattonnay, G.; Brubach, J. B.; Huntz, A. M.; Tétot, R. Experimental and ab initio infrared study of χ-, κ-and α-aluminas formed from gibbsite. *J. Solid State Chem.* **2010**, *183*, 901−908.
(42) Xu, L.; Song, H.; Chou, L. Facile synthesis of nano-crystalline alpha-alumina at low temperature via an absolute ethanol sol−gel strategy. *Mater. Chem. Phys.* **2012**, *132*, 1071−1076.
(43) Lin, Z.; Scriven, L. E.; Davis, H. T. Cryogenic electron microscopy of rodlike or wormlike micelles in aqueous solutions of nonionic surfactant hexaethylene glycol monohexadecyl ether. *Langmuir* **1992**, *8*, 2200−2205.
(44) Zhu, H. Y.; Riches, J. D.; Barry, J. C. γ-alumina nanofibers prepared from aluminum hydrate with poly (ethylene oxide) surfactant. *Chem. Mater.* **2002**, *14*, 2086−2093.
(45) Liu, Y.; Ma, D.; Han, X.; Bao, X.; Frandsen, W.; Wang, D.; Su, D. Hydrothermal synthesis of microscale boehmite and gamma nanoleaves alumina. *Mater. Lett.* **2008**, *62*, 1297−1301.
(46) Das, P. P.; Samanta, S.; Blom, D. A.; Pramanik, S.; Devi, P. S.; Vogt, T.; Lee, Y. Pressure-induced assemblies and structures of graphitic-carbon sheet encapsulated Au nanoparticles. *Nanoscale* **2020**, *12*, 17462−17469.

https://dx.doi.org/10.1021/acsomega.0c05541
ACS Omega 2021, 6, 4740−4748

(47) Donoeva, B.; Masoud, N.; De Jongh, P. E. Carbon support surface effects in the gold-catalyzed oxidation of 5-hydroxymethylfurfural. *ACS Catal.* **2017**, *7*, 4581−4591.
(48) Xu, S.; Zhou, P.; Zhang, Z.; Yang, C.; Zhang, B.; Deng, K.; Bottle, S.; Zhu, H. Selective oxidation of 5-hydroxymethylfurfural to 2, 5-furandicarboxylic acid using O_2 and a photocatalyst of Co-thioporphyrazine bonded to g-C_3N_4. *J. Am. Chem. Soc.* **2017**, *139*, 14775−14782.
(49) Bronnimann, C.; Bodnar, Z.; Hug, P.; Mallat, T.; Baiker, A. Direct oxidation of L-sorbose to 2-keto-L-gulonic acid with molecular oxygen on platinum-and palladium-based catalysts. *J. Catal.* **1994**, *150*, 199−211.
(50) Mei, N.; Liu, B.; Zheng, J.; Lv, K.; Tang, D.; Zhang, Z. A novel magnetic palladium catalyst for the mild aerobic oxidation of 5-hydroxymethylfurfural into 2, 5-furandicarboxylic acid in water. *Catal. Sci. Technol.* **2015**, *5*, 3194−3202.
(51) Rass, H. A.; Essayem, N.; Besson, M. Selective aqueous phase oxidation of 5-hydroxymethylfurfural to 2, 5-furandicarboxylic acid over Pt/C catalysts: influence of the base and effect of bismuth promotion. *Green Chem.* **2013**, *15*, 2240−2251.
(52) Wu, L.; Moteki, T.; Gokhale, A. A.; Flaherty, D. W.; Toste, F. D. Production of fuels and chemicals from biomass: condensation reactions and beyond. *Chem* **2016**, *1*, 32−58.
(53) Ci, J.; Cao, C.; Kuga, S.; Shen, J.; Wu, M.; Huang, Y. Improved performance of microbial fuel cell using esterified corncob cellulose nanofibers to fabricate air-cathode gas diffusion layer. *ACS Sustainable Chem. Eng.* **2017**, *5*, 9614−9618.
(54) Biella, S.; Prati, L.; Rossi, M. Gold catalyzed oxidation of aldehydes in liquid phase. *J. Mol. Catal. A: Chem.* **2003**, *197*, 207−212.
(55) Della Pina, C.; Falletta, E.; Prati, L.; Rossi, M. Selective oxidation using gold. *Chem. Soc. Rev.* **2008**, *37*, 2077−2095.
(56) Su, H.; Zhang, K.-X.; Zhang, B.; Wang, H.-H.; Yu, Q.-Y.; Li, X.-H.; Antonietti, M.; Chen, J.-S. Activating cobalt nanoparticles via the Mott−Schottky effect in nitrogen-rich carbon shells for base-free aerobic oxidation of alcohols to esters. *J. Am. Chem. Soc.* **2017**, *139*, 811−818.
(57) Shang, C.; Liu, Z.-P. Origin and activity of gold nanoparticles as aerobic oxidation catalysts in aqueous solution. *J. Am. Chem. Soc.* **2011**, *133*, 9938−9947.
(58) Staykov, A.; Nishimi, T.; Yoshizawa, K.; Ishihara, T. Oxygen activation on nanometer-size gold nanoparticles. *J. Phys. Chem. C* **2012**, *116*, 15992−16000.
(59) Wolski, L.; Sobczak, I.; Ziolek, M. Variability of surface components in gold catalysts−The role of hydroxyls and state of gold on activity and selectivity of Au-Nb2O5 and Au-$ZnNb_2O_6$ in methanol oxidation. *J. Catal.* **2017**, *354*, 100−112.
(60) Majumdar, B.; Bhattacharya, T.; Sarma, T. K. Gold Nanoparticle−Polydopamine−Reduced Graphene Oxide Ternary Nanocomposite as an Efficient Catalyst for Selective Oxidation of Benzylic C (sp^3)− H Bonds Under Mild Conditions. *ChemCatChem* **2016**, *8*, 1825−1835.
(61) Zope, B. N.; Hibbitts, D. D.; Neurock, M.; Davis, R. J. Reactivity of the gold/water interface during selective oxidation catalysis. *Science* **2010**, *330*, 74−78.
(62) Han, P.; Tana, T.; Xiao, Q.; Sarina, S.; Waclawik, E. R.; Gómez, D. E.; Zhu, H. Promoting Ni (II) catalysis with plasmonic antennas. *Chem* **2019**, *5*, 2879−2899.

https://dx.doi.org/10.1021/acsomega.0c05541
ACS Omega 2021, 6, 4740−4748